J. Fluid Mech. (1990), *vol.* 215, *pp.* 431–455
Printed in Great Britain

On the shearing flow of foams and concentrated emulsions

By DOUGLAS A. REINELT[1] AND ANDREW M. KRAYNIK[2]

[1] Department of Mathematics, Southern Methodist University, Dallas, TX 75275, USA

[2] Fluid and Thermal Sciences Department, Division 1511 Sandia National Laboratories, Albuquerque, NM 87185, USA

(Received 11 April 1989 and in revised form 13 October 1989)

Shearing flow of an idealized, two-dimensional foam with monodisperse, spatially periodic cell structure is examined. Viscous effects are modelled by the film withdrawal mechanism of Mysels, Shinoda & Frankel. The primary flow occurs where thin films with inextensible interfaces are withdrawn from or recede into quasi-static Plateau borders, film junctions that contain most of the liquid. The viscous flow induces an excess tension that varies between films and alters the foam structure. The instantaneous structure and macroscopic stress for a foam of arbitrary orientation are determined for simple shearing and planar extensional flow. As the foam flows, the Plateau borders coalesce and separate, which leads to switching of bubble neighbours. The quasi-steady asymptotic analysis of the flow is valid for small capillary numbers Ca based on the macroscopic deformation rate. This requires the foam to be wet, i.e. the liquid volume fraction must be large enough that structure varies continuously with strain. The viscous contribution to the instantaneous stress is $O(Ca^{\frac{2}{3}})$ and depends on the foam orientation and liquid content. Viscometric functions are determined by time averaging the instantaneous stress. When these functions are scaled by surface tension over cell size, the shear stress is $O(Ca^{\frac{2}{3}})$; by contrast, the first normal stress difference is $O(1)$. Even though wet foams are elastic for small but finite deformations, the time-averaged shear stress does not evidence a yield stress.

1. Introduction

The development of microrheological theories for dilute fluid–fluid dispersions is facilitated by the absence of hydrodynamic interaction between drops that are nearly spherical in shape (Taylor 1932, 1954; Schowalter, Chaffey & Brenner 1968; Cox 1969; Frankel & Acrivos 1970; Schowalter 1978; Flumerfelt 1980). The shear rheology of dilute dispersions can be expressed as a small perturbation on the Newtonian behaviour of the continuous phase. By contrast, it is even difficult to quantify the equilibrium shape of the phases for highly concentrated dispersions. Foams consist of polyhedral gas bubbles separated by a continuous network of thin non-planar liquid films; concentrated liquid–liquid emulsions are similar in structure. Moreover, foams and concentrated emulsions exhibit solid-like characteristics such as a finite shear modulus and yield stress, in addition to non-Newtonian viscosity and slip at the wall.

The rheology of these concentrated systems is similar when compressibility and viscosity of the dispersed phase can be neglected. Here, we consider such conditions

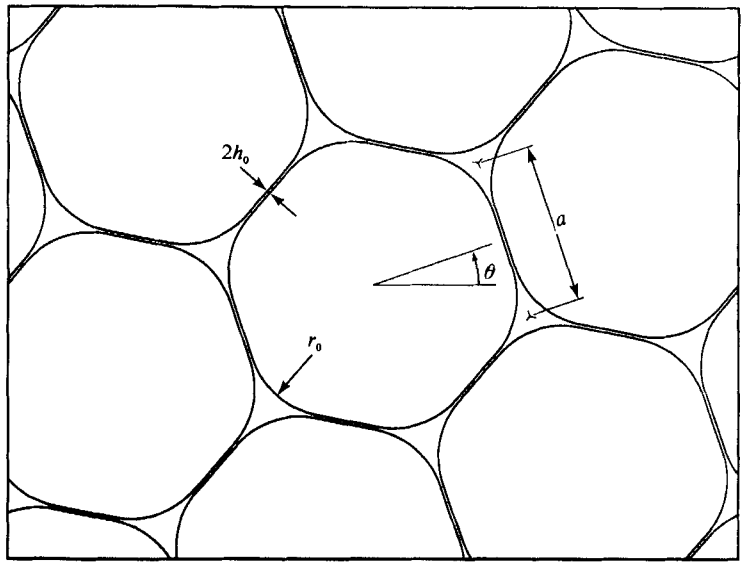

FIGURE 1. The equilibrium structure of an idealized two-dimensional foam with perfectly ordered, monodisperse, cell structure. Shown are thin films with thickness $2h_0$, Plateau borders with uniform curvature r_0, the characteristic cell size a, and the initial orientation angle θ.

and refer to all of these highly structured fluids as foams. Previous experimental and theoretical studies of foam rheology have been reviewed by Kraynik (1988).

Even though Kelvin (1887) described the shape of an ideal foam cell over a century ago, no microrheological model based on three-dimensional structure has been developed. Kelvin's minimal tetrakaidecahedron contains six planar quadrilateral and eight non-planar hexagonal faces, all with curved edges. Because of this geometrical complexity, all theories developed over the past decade have assumed two-dimensional structure. These models are useful and represent logical steps toward more complete theories. Although there has been progress in the computer simulation of two-dimensional, polydisperse foams with disordered structure (Weaire & Kermode 1983, 1984; Weaire, Fu & Kermode 1986; Weaire & Fu 1988), we and most other investigators follow Princen (1983) and consider perfectly ordered systems.

The theories for monodisperse foams examine deformations of the equilibrium structure shown in figure 1. The characteristic parameters include cell size a, film thickness $2h_0$, radius r_0 of the Plateau border, and liquid volume fraction ϕ. The presence of a surface-active agent that gives rise to a positive disjoining pressure Π promotes foam stability. The collective fluid microstructure forces in thin films, which stem from molecular, ionic–electrostatic, and steric interaction effects, determine Π. A balance between capillary pressure in the Plateau borders and disjoining pressure in the thin films determines the equilibrium distribution of liquid between these two regions. Because the disjoining pressure is typically effective over very small distances, we restrict our attention to foams where $h_0 \ll r_0$ and assume that essentially all of the liquid is confined initially to the Plateau borders.

In the following analysis, we determine the response of a monodisperse foam in slow, steady shearing flows. Our model foam exhibits nonlinear elastic behaviour for small but finite deformations. Under large strain, the length of a thin film can go to zero, resulting in coalescence of Plateau borders. The eventual separation of the

borders produces a new film, provides a mechanism for switching of cell neighbours, and reduces distortion of the dispersed phase. This coalescence and separation of Plateau borders is a fundamental mechanism for foam flow. Small deformation theories (Schwartz & Princen 1987; Reinelt & Kraynik 1989) do not incorporate this mechanism and cannot describe steady flow.

When the foam is deformed, thin films connecting Plateau borders change length. Film expansion causes liquid to be withdrawn from the Plateau borders and redistributed into the films. To model viscous effects, we adopt the film withdrawal mechanism described by Mysels, Shinoda & Frankel (1959) who examined the steady withdrawal and recession of thin film from an otherwise stagnant pool of liquid. Their assumption that thin-film interfaces are inextensible leads to withdrawn film surface tensions that exceed the equilibrium value T_0.

The matched asymptotic analysis of Mysels *et al.* is developed for small capillary numbers based on film withdrawal speed. To ensure that the capillary number associated with each film in the foam is always small, our quasi-steady analysis is restricted to small macroscopic strain rates and to 'wet' foams. A wet foam contains enough liquid to guarantee slow film withdrawal speeds during coalescence and separation of Plateau borders.

The detailed variation in foam structure and film-level transport with imposed flow determines the instantaneous macroscopic rheology of the foam. To calculate viscometric functions such as the viscosity and first normal stress difference for these perfectly ordered fluids, the instantaneous stress is averaged over a suitable time. This can be accomplished for initial foam orientations, called strain periodic (Kraynik & Hansen 1986, 1987) or reproducible (Adler & Brenner 1985), for which the foam structure is a periodic function of strain. In addition to simple shear, we also examine planar extensional flow and calculate extensional viscosity.

2. Mathematical formulation

The rheology of a two-dimensional monodisperse foam can be analysed by examining the response of the unit cell, shown in figure 2, to homogeneous deformations (Princen 1983; Khan & Armstrong 1986, 1987; Kraynik & Hansen 1986, 1987; Reinelt & Kraynik 1989). For simple shearing flow, the area (volume per unit depth) of the unit cell is constant and given by $A = 3^{\frac{3}{2}}a^2/4$. The displacement of each film midpoint is affine and determined from the macroscopic strain. The vectors $\boldsymbol{b}_k$ ($k = 1, 2$) represent the position of the kth film midpoint relative to the midpoint of film 3. For simple shear, these vectors are

$$\boldsymbol{b}_k = (b^0_{kX} + \gamma b^0_{kY}, b^0_{kY}) = \boldsymbol{g}_k - \boldsymbol{g}_3, \tag{2.1}$$

where (b^0_{kX}, b^0_{kY}) are the components of $\boldsymbol{b}_k$ when the shear strain γ is equal to zero. The vectors $\boldsymbol{g}_k = G_k(\cos\beta_k, \sin\beta_k)$ ($k = 1, 2, 3$) represent the length G_k and orientation of each film in the unit cell. The angle β_k is measured counterclockwise from the positive X-axis as shown in figure 3. For an undeformed foam, the film variables are

$$G^0_k = \tfrac{1}{2}a, \quad \beta^0_1 = \theta + \tfrac{1}{2}\pi, \quad \beta^0_2 = \theta + \tfrac{11}{6}\pi, \quad \beta^0_3 = \theta + \tfrac{7}{6}\pi, \tag{2.2}$$

where θ represents the initial orientation of the foam as shown in figure 1.

The thin films connect junction regions called Plateau borders whose geometry is shown in figure 3. In our quasi-steady analysis, the pressure is uniform throughout the border and is given by $p = p_0 - T_0/r$; where p_0 is the uniform pressure in the dispersed phase, T_0 is the equilibrium surface tension, and r is the uniform radius of

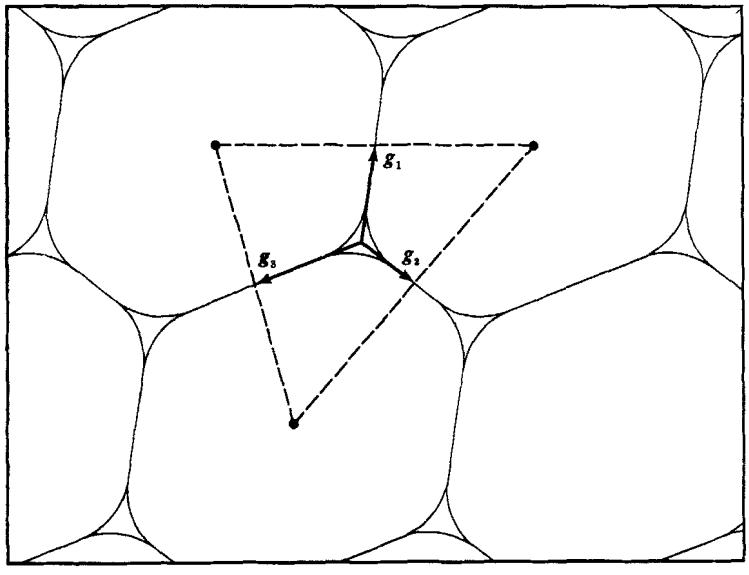

FIGURE 2. A unit cell and the film vectors $\boldsymbol{g}_k$ are shown for a deformed foam. The film-midpoint position vectors are given by $\boldsymbol{b}_k = \boldsymbol{g}_k - \boldsymbol{g}_3$.

curvature in the border. The quantity D_k in figure 3 is the distance from the centre to the mouth of the Plateau border and $2rd_k$ is the distance across the mouth; both lengths can vary with k. From the border geometry, law of sines, etc. we get the following equations, which will be used later in the analysis,

$$(1+d_1)\sin\alpha_2 = (1+d_2)\sin\alpha_1, \tag{2.3}$$

$$(1+d_3) = (1+d_1)\cos\alpha_2 + (1+d_2)\cos\alpha_1, \tag{2.4}$$

$$D_k = r(1+d_k)\cot\alpha_k. \tag{2.5}$$

The first two equations remain valid when indices are permuted. The angles α_k and β_k are related through permutations of

$$\beta_3 - \beta_1 = \pi - \alpha_2. \tag{2.6}$$

The Plateau border is bounded by circles of radius r that are centred at the corners of the (dash-dotted) triangle in figure 3. The area of the Plateau border is given by

$$A_{\mathrm{PB}} = 2r^2(1+d_1)(1+d_2)\sin\alpha_3 - \tfrac{1}{2}\pi r^2. \tag{2.7}$$

Again, these indices can be permuted. For an undeformed foam, $d_k = 0, \alpha_k = \frac{1}{3}\pi$, and

$$A^0_{\mathrm{PB}} = \sqrt{3}\, r_0^2 - \tfrac{1}{2}\pi r_0^2. \tag{2.8}$$

The equilibrium radius r_0 is determined from $A^0_{\mathrm{PB}} = \phi A$, where A is the area of the unit cell and ϕ is the liquid volume fraction. When the foam is being deformed, r is determined from conservation of mass,

$$A_{\mathrm{PB}} + A_{\mathrm{TF}} = A^0_{\mathrm{PB}}, \tag{2.9}$$

where A_{TF} is the total area of the thin films which is negligible in the undeformed state or under static conditions.

To determine an equation for the shape of the interface in the border and later in

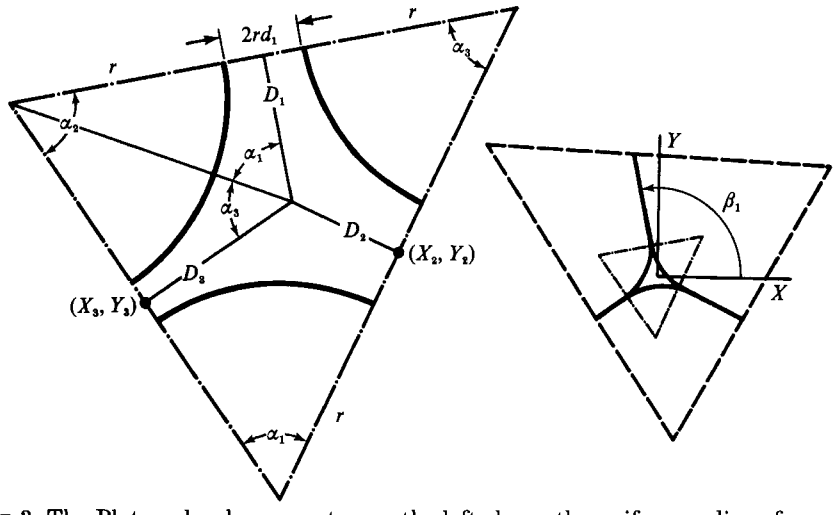

FIGURE 3. The Plateau border geometry on the left shows the uniform radius of curvature r and the distances D_k. The position (X_k, Y_k) indicates the origin of each film-level coordinate system shown in figure 4. The distance across each mouth is $2rd_k$; this length is $O(Ca^{\frac{2}{3}})$ when there is a thin film and $O(1)$ when film k has disappeared through Plateau border coalescence. The insert on the right shows the relative position of the Plateau border in the unit cell and the orientation angle β_1 of film 1.

the thin films, we switch from the global coordinate system (X, Y) centred in the Plateau border, to a local coordinate system (x, y). This film-level coordinate system is centred at the Plateau border mouth (X_k, Y_k) with the x-axis aligned along the kth film. The transformation between the coordinate systems is

$$X = X_k + x\cos\beta_k - y\sin\beta_k, \quad Y = Y_k + x\sin\beta_k + y\cos\beta_k. \tag{2.10}$$

In terms of the local coordinates, interfaces in the Plateau border are described by $y = \pm h(x)$ where

$$h(x) = r(1+d_k) - (r^2 - x^2)^{\frac{1}{2}}. \tag{2.11}$$

On each side of the Plateau border triangle, the effective tension is $2T_k$, where

$$T_k = T_0/(1+h_x^2)^{\frac{1}{2}} + hT_0/r = T_0(1+d_k), \tag{2.12}$$

and h_x is the derivative of h with respect to x. The first term in the middle expression is the component of tension parallel to $\boldsymbol{g}_k$ and the second term stems from the capillary pressure difference between the two phases; the right-hand side follows from (2.11). Using (2.3), (2.4), (2.6) and (2.12), one can verify that a force balance on the Plateau border is satisfied,

$$\sum_{k=1}^{3} T_k \boldsymbol{p}_k = \boldsymbol{0}, \tag{2.13}$$

where $\boldsymbol{p}_k = (\cos\beta_k, \sin\beta_k)$ is the unit vector parallel to $\boldsymbol{g}_k$.

We develop an analysis for small imposed strain rate $\dot{\gamma}$ by expanding all variables for $Ca \ll 1$, where $Ca = \mu a\dot{\gamma}/T_0$ is the macroscopic capillary number. The primary flow occurs where thin film is withdrawn from the Plateau border. In solving the equations that govern this flow, Mysels *et al.* (1959) showed that the withdrawn film thickness, the excess film tension, etc. are $O(Ca^{\frac{2}{3}})$. Knowing this, our expansions take the form,

$$G_k = \hat{G}_k + Ca^{\frac{2}{3}} G'_k, \tag{2.14}$$

where the ˆ denotes a quasi-static term and the prime refers to rate dependence. Both the hat and prime variables are functions of the strain γ. When film is slowly withdrawn, the distance across the mouth of the border is $O(Ca^{\frac{2}{3}})$; because $\hat{d}_k = 0$ each thin film has length

$$L_k = G_k - D_k. \tag{2.15}$$

The withdrawal speed of individual films is approximated by $U_k = \dot{\gamma}\, \mathrm{d}\hat{L}_k/\mathrm{d}\gamma$. This provides the connection between each film-level capillary number Ca_k and the macroscopic capillary number:

$$Ca_k = \mu U_k/T_0 = Ca\, F_k, \quad \text{where} \quad aF_k = \mathrm{d}\hat{L}_k/\mathrm{d}\gamma. \tag{2.16}$$

A more complete discussion of film-level flow is given in the next section.

To fully determine the evolution of foam structure for large strains, one must account for the complete disappearance of a film and the subsequent border coalescence. Following Princen (1983) a Plateau border connected by three thin films to its neighbours is labelled as mode I. A transition from mode I to mode II occurs when the length of one connecting film becomes zero. In mode II, two Plateau borders are coalesced; thus, $\hat{d}_k \neq 0$ for a single value of k. All borders form pairs simultaneously in a monodisperse spatially periodic foam. A third possibility, not encountered in previous work, occurs when two of the thin films have vanished. For this case, which we refer to as mode III, our foam consists of compressed layers of bubbles separated by channels of fluid. These three modes are described in detail later. The values of γ at which the mode transitions occur are strongly dependent upon the initial orientation angle θ and liquid volume fraction ϕ of the foam.

In addition to mode transitions, it is necessary to account for switching of bubble neighbours by redefining the unit cell when $G_k = 0$, for some value of k. The new reference vectors $\boldsymbol{b}_k^0$, described in (2.1), which determine the new unit cell, are specified in terms of the current $\boldsymbol{b}_k$ in the following manner (Kraynik & Hansen 1986):

$$\left.\begin{aligned} &\text{if } G_1 = 0, \quad \text{then } \boldsymbol{b}_1^0 = \boldsymbol{b}_1, \quad \boldsymbol{b}_2^0 = \boldsymbol{b}_2 - \boldsymbol{b}_1, \\ &\text{if } G_2 = 0, \quad \text{then } \boldsymbol{b}_1^0 = \boldsymbol{b}_1 - \boldsymbol{b}_2, \quad \boldsymbol{b}_2^0 = \boldsymbol{b}_2, \\ &\text{if } G_3 = 0, \quad \text{then } \boldsymbol{b}_1^0 = \boldsymbol{b}_2, \quad \boldsymbol{b}_2^0 = \boldsymbol{b}_1. \end{aligned}\right\} \tag{2.17}$$

When the unit cell is redefined, the 'incremental' strain in (2.1) is set to zero. In general, there are many mode transitions and unit cell switches as the foam flows. Through this mechanism, the distortion of individual bubbles can be bounded even when the relative displacement of two bubble centres is arbitrarily large.

3. Film-level viscous flow

This flow was analysed by Mysels *et al.* (1959) and adapted to foams by Schwartz & Princen (1987). The matched asymptotic analysis is developed for small Ca_k but neglects disjoining pressure; this means that the results are not valid in the limit $Ca_k \to 0$ (Mysels & Cox 1962; Lyklema, Scholten & Mysels 1965; Teletzke, Davis & Scriven 1988). Essential features of this quasi-steady analysis are now described.

The primary flow occurs where a thin film with inextensible interfaces is withdrawn from or recedes into the Plateau border. Figure 4 shows an enlarged view of a thin film near the Plateau border and defines the geometry in terms of the film-level coordinate system of (2.10). The film thickness profile in region III is determined by the withdrawal speed of each film segment from the border. The viscous flow that tends to equalize the film thickness in region III is neglected. The

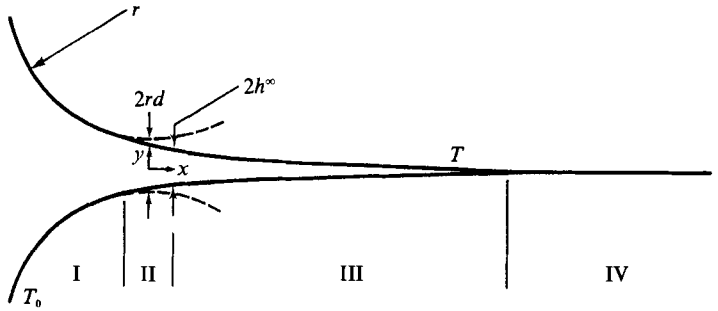

FIGURE 4. Enlarged view of a thin film near the Plateau border (I) showing the regions identified by Schwartz & Princen to be significant in a quasi-steady analysis of film-level flow. The primary flow occurs in the transition region (II) and determines the thickness h^∞ of film entering the withdrawn film region (III). The very small thickness of equilibrium film in region IV is determined by disjoining pressure. In this analysis, the equilibrium surface tension T_0 in the Plateau border differs from the uniform value of surface tension T in regions III and IV. Subscripts associated with individual films on d, h^∞, and T have been omitted.

equilibrium film thickness in region IV is also neglected. Films that are generated by separation of Plateau borders during shearing flow will not have a region IV.

Viscous flow in the transition region (II) determines both d'_k and the thickness of film entering region III. The appropriate lubrication form of the Stokes equations is,

$$u_x + v_y = 0, \quad p_x = \mu u_{yy}, \quad p_y = 0. \tag{3.1}$$

The boundary conditions, $u = U_k$ and $v = U_k h_x$, apply on the interface $y = h(x)$. Symmetry at the centreline requires: $u_y = 0$ and $v = 0$. The pressure only depends on x and is determined from the local curvature: $p = p_0 - T_0 h_{xx}$.

A similarity solution for the transition region satisfies the differential equation

$$\eta_{\xi\xi\xi} = (\eta - 1)/\eta^3. \tag{3.2}$$

where $$h = h_k^\infty \eta, \quad x = -h_k^\infty \xi (3Ca_k)^{-\frac{1}{3}}, \quad Ca_k = \mu U_k / T_0.$$

Here, h_k^∞ is the asymptotic thickness of film withdrawn from the transition region. Discussion of the matched asymptotic analysis and numerical integration of (3.2) can be found elsewhere (Landau & Levich 1942; Mysels *et al.* 1959; Bretherton 1961; Park & Homsy 1984; Schwartz & Princen 1987; Reinelt & Kraynik 1989).

The results that are relevant to our problem describe the asymptotic film thickness

$$h_k^\infty = r P_k (3Ca_k)^{\frac{2}{3}} \quad \text{or } h'_k = \hat{r} P_k (3F_k)^{\frac{2}{3}}, \tag{3.3}$$

and the distance separating interfaces in the Plateau border

$$d_k = R_k h_k^\infty / r = P_k R_k (3Ca_k)^{\frac{2}{3}} \quad \text{or } d'_k = P_k R_k (3F_k)^{\frac{2}{3}}, \tag{3.4}$$

where F_k is defined in (2.16) and the coefficients P_k and R_k are determined by solving (3.2).

It is also necessary to calculate the area of each thin film. The time rate of change of this area is

$$\dot{A}_k = 2U_k h_k^\infty = 2(a\dot{\gamma} F_k)(Ca^{\frac{2}{3}} h'_k), \tag{3.5}$$

which integrates to $$A'_k = 2a3^{\frac{2}{3}} \int \hat{r} P_k (F_k)^{\frac{5}{3}} \mathrm{d}\gamma. \tag{3.6}$$

By summing the area of the thin films, we determine $A_{\mathrm{TF}} = Ca^{\frac{2}{3}} A'_{\mathrm{TF}}$.

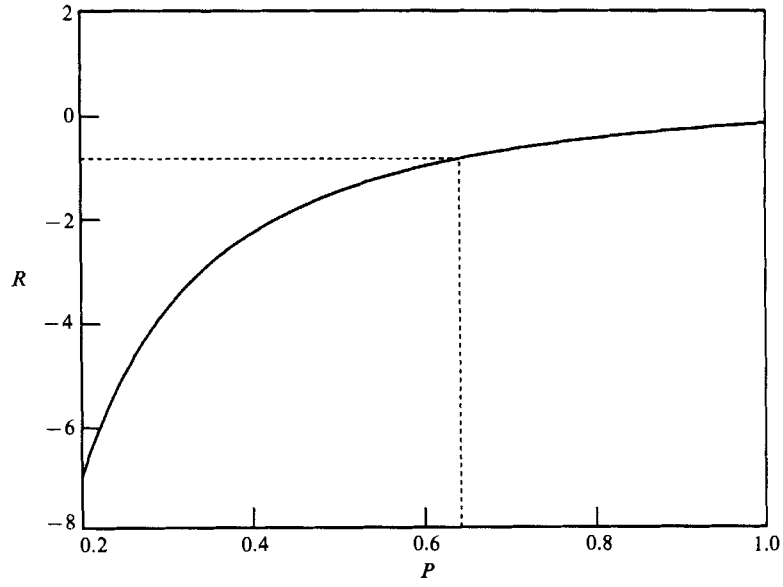

FIGURE 5. Coefficients P and R used to determine excess tension for a receding film. The indicated values apply when a film recedes at the same speed and thickness at which it was withdrawn ($P = 0.6430$, $R = -0.8452$).

When a film is being withdrawn from the border, $F_k > 0$, and the coefficients

$$P_k = 0.6430, \quad R_k = 2.8996, \tag{3.7}$$

are uniquely determined. In this case, h'_k and A'_k are calculated and stored as functions of each thin film length $\hat{L}_k$. When a film is receding into the border, its thickness and remaining area are given by these stored quantities. Knowing h'_k and the values of $\hat{r}$ and F_k, the value of P_k is determined from (3.3). The value of R_k is obtained by integrating the differential equation (3.2). Figure 5 shows R_k as a function of P_k for a receding film over the range $0.2 < P_k < 1.0$. The integration was done using the subroutine D02HBF in the NAG FORTRAN Library.

4. Instantaneous macroscopic stress tensor

The instantaneous macroscopic stress for the foam is calculated by averaging the local stress over the unit cell (Batchelor 1970). The equation for the effective stress can be written for our two-dimensional foam as

$$\boldsymbol{\sigma} = \frac{1}{A}\left[\int_A \tilde{\boldsymbol{\sigma}}\,\mathrm{d}a + \int_S T\boldsymbol{t}\boldsymbol{t}\,\mathrm{d}s\right], \tag{4.1}$$

where

$$\tilde{\boldsymbol{\sigma}} = -p\boldsymbol{I} + \mu[\boldsymbol{\nabla u} + (\boldsymbol{\nabla u})^{\dagger}].$$

Here, $\tilde{\boldsymbol{\sigma}}$ is the local instantaneous stress, A is the area of the unit cell, S is the interface that separates the two phases, T is the surface tension which may be non-uniform, and $\boldsymbol{t}$ is a unit vector that is tangent to the interface.

To the order of our analysis, contributions to the stress from the first integral in (4.1) are isotropic and equal to $[-p_0 + (T_0/r)(A_{\mathrm{PB}}/A)]\boldsymbol{I}$. These terms come from the bubble pressure p_0 and the capillary pressure in the Plateau border. It may be

surprising that the contribution from viscous flow in the transition region to the first integral is higher order and can be neglected.

The border contribution from the second integral is also isotropic and equal to $(\pi r T_0/2A)\boldsymbol{I}$. All anisotropic terms come from the thin film interfaces. For each thin film interface, we approximate the tangent vector $\boldsymbol{t}$ by the unit vector $\boldsymbol{p}_k = (\cos\beta_k, \sin\beta_k)$ and the surface tension T by T_k from (2.12). Reinelt & Kraynik (1989) have shown that these approximations contain all terms relevant to this analysis. The contribution to the stress tensor from all the thin films is given by,

$$\boldsymbol{\sigma}_{\mathrm{TF}} = \frac{2}{A}\sum_{k=1}^{3} T_k L_k \boldsymbol{p}_k \boldsymbol{p}_k. \tag{4.2}$$

The instantaneous shear stress and first normal stress difference for the foam are

$$\sigma_{XY} = \frac{T_0}{A}\sum_{k=1}^{3}(1+d_k)L_k \sin 2\beta_k,$$

$$N_1 = \sigma_{XX} - \sigma_{YY} = \frac{2T_0}{A}\sum_{k=1}^{3}(1+d_k)L_k \cos 2\beta_k. \tag{4.3}$$

5. Evaluation of the foam structure

Princen (1983) completely determined the quasi-static foam structure as a function of strain for the initial orientation $\theta = 0$. For this particular case, Plateau border coalescence only involves pairing and the structure is a periodic function of strain. For small liquid volume fractions ϕ the solutions exhibit turning points and corresponding discontinuities. However, when the foam is sufficiently wet, foam structure is a continuous function of strain. Princen's results for the structure of a wet foam are reproduced in figure 6. The shear stress is shown in figure 7 for several values of the dispersed phase volume fraction $\phi_{\mathrm{d}} = 1-\phi$. The limiting value $\phi_{\mathrm{d}} = 0.9069$ represents close-packed circular bubbles. The dashed lines indicate discontinuities in stress which result from discontinuities in foam structure.

This analysis extends previous work (Princen 1983; Khan 1985; Pacetti 1985; Kraynik & Hansen 1986; Khan & Armstrong 1989; Reinelt & Kraynik 1989) by accounting for viscous effects in arbitrarily large shearing deformations. The approach is valid for all initial orientations of the foam but we restrict ourselves to considering values of ϕ that provide continuous quasi-static solutions.

The next four subsections describe how all variables that represent the foam structure are determined to $O(Ca^{\frac{2}{3}})$. This includes both the film network and the Plateau border structure. One can forgo these algebraic details and skip to §6 without losing continuity.

5.1. *Quasi-static mode I problem*

The mode I problem for an undeformed foam of arbitrary initial orientation was solved by Khan & Armstrong (1986). We extend their quasi-static analysis to arbitrary reference configurations.

Because the surface tension is uniform to leading order, three thin films are separated by equal angles of $\frac{2}{3}\pi$ and the Plateau border exhibits equilibrium structure. This implies that

$$\hat{d}_k = 0, \quad \hat{D}_k = \hat{r}/\sqrt{3} = r_0/\sqrt{3}, \quad \hat{\alpha}_k = \tfrac{1}{3}\pi. \tag{5.1}$$

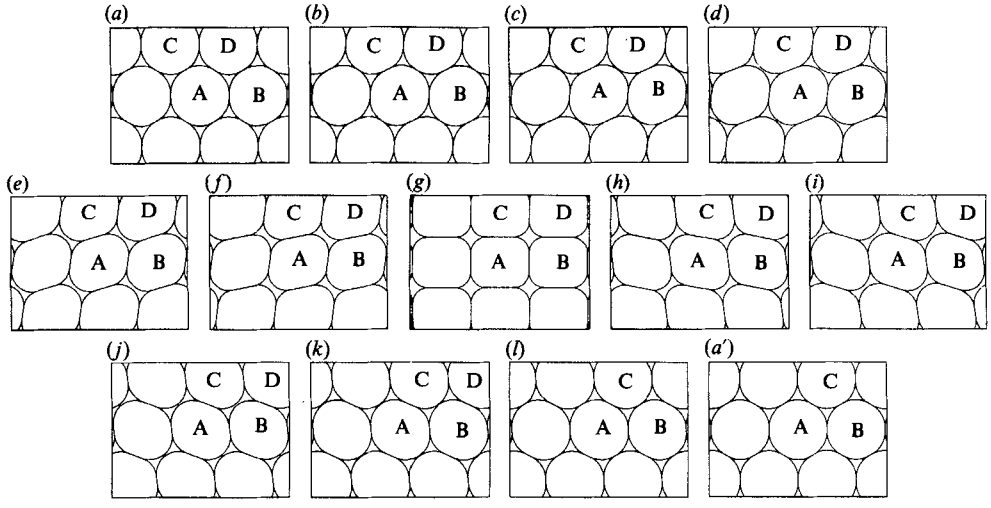

FIGURE 6. Evolution of foam structure with strain for simple shear with $\theta = 0$ and $\phi = 0.07$. The range of shear strain is $2/\sqrt{3}$ with equal increments.

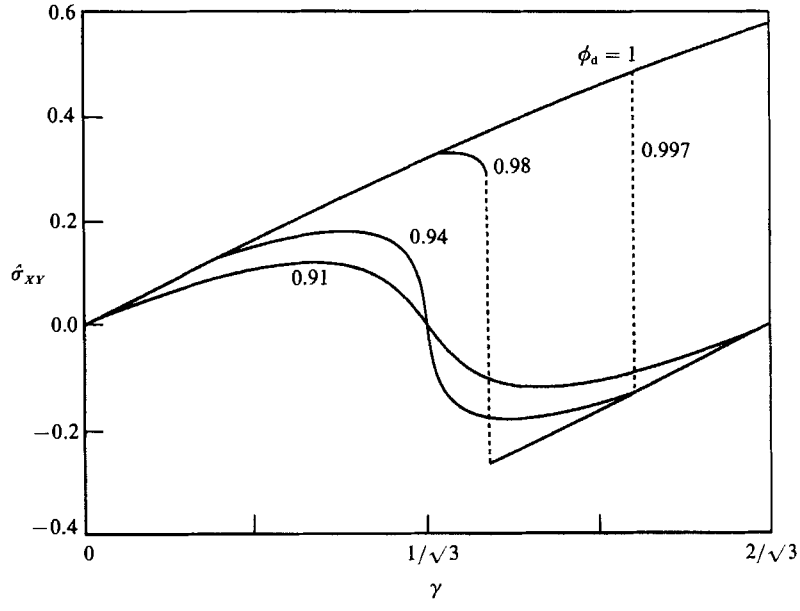

FIGURE 7. Quasi-static shear stress *vs.* strain curves corresponding to two regimes of dispersed-phase volume fraction ϕ_d with $\theta = 0$. When $\phi_d < \phi_d^* \approx 0.9466$, the shear stress is antisymmetric about $\gamma = 1/\sqrt{3}$ and changes in foam structure are continuous. When $\phi_d > \phi_d^*$, changes in foam structure are abrupt, as indicated by the dashed line. The stress has been scaled by T_0/a.

To determine mode I film lengths and orientations, we take the dot product of $\boldsymbol{p}_3$ with (2.1) and obtain

$$-G_3 = G_1 \cos\alpha_2 + a_1 = G_2 \cos\alpha_1 + a_2, \tag{5.2}$$

where

$$a_k = b_{kX} \cos\beta_3 + b_{kY} \sin\beta_3.$$

Taking the cross product of $\boldsymbol{p}_3$ with (2.1) provides

$$G_1 \sin\alpha_2 = e_1, \quad G_2 \sin\alpha_1 = -e_2, \tag{5.3}$$

where $$e_k = b_{kX}\sin\beta_3 - b_{kY}\cos\beta_3.$$

Combining (5.2) and (5.3) leads to an equation for the angle β_3

$$e_1\cot\alpha_2 + a_1 = -e_2\cot\alpha_1 + a_2. \tag{5.4}$$

To leading order,
$$\left.\begin{aligned} \tan\hat{\beta}_3 &= \frac{b_{1Y}+b_{2Y}+\sqrt{3}(b_{2X}-b_{1X})}{b_{1X}+b_{2X}+\sqrt{3}(b_{1Y}-b_{2Y})}, \\ \hat{\beta}_1 &= \hat{\beta}_3 - \tfrac{2}{3}\pi, \quad \hat{\beta}_2 = \hat{\beta}_3 + \tfrac{2}{3}\pi. \end{aligned}\right\} \tag{5.5}$$

The film lengths are now determined from (5.2) and (5.3) and are given by

$$\hat{G}_1 = 2\hat{e}_1/\sqrt{3}, \quad \hat{G}_2 = -2\hat{e}_2/\sqrt{3}, \quad \hat{G}_3 = -\hat{G}_1/2 - \hat{a}_1. \tag{5.6}$$

For the special case of an initially undeformed foam in simple shear,

$$\begin{aligned} \hat{\beta}_k &= \beta_k^0 - \tan^{-1}(\tfrac{1}{2}\gamma), \\ \hat{G}_k &= \tfrac{1}{4}a[(4+\gamma^2)^{\frac{1}{2}} + 2\gamma\sin\psi_k], \end{aligned} \tag{5.7}$$

where $$\psi_k = 2\beta_k^0 - \tan^{-1}(\tfrac{1}{2}\gamma).$$

5.2. *Quasi-static mode II problem*

The transition from mode I to mode II occurs when the length of one thin film goes to zero. We assume $L_3 = G_3 - D_3 = 0$; the other two cases are identical with permutation of indices. Taking the dot product of $\boldsymbol{p}_k$ $(k = 1, 2)$ with (2.1) gives

$$G_1 = -G_3\cos\alpha_2 + c_1, \quad G_2 = -G_3\cos\alpha_1 + c_2, \tag{5.8}$$

where $$c_k = b_{kX}\cos\beta_k + b_{kY}\sin\beta_k.$$

By taking the cross product of $\boldsymbol{p}_k$ $(k = 1, 2)$ with (2.1) and using (2.3) and (2.5) we get

$$\begin{aligned} f_1 &= G_3\sin\alpha_2 = D_3\sin\alpha_2 = r(1+d_2)\cos\alpha_3, \\ -f_2 &= G_3\sin\alpha_1 = D_3\sin\alpha_1 = r(1+d_1)\cos\alpha_3, \end{aligned} \tag{5.9}$$

where $$f_k = b_{kX}\sin\beta_k - b_{kY}\cos\beta_k.$$

When only film 3 has vanished, $\hat{d}_1$ and $\hat{d}_2$ are still equal to zero. Since the area of the thin film is $O(Ca^{\frac{2}{3}})$, (2.7) and (2.9) reduce to

$$\hat{A}_{\mathrm{PB}} = 2\hat{r}^2\sin\hat{\alpha}_3 - \tfrac{1}{2}\pi\hat{r}^2 = A_{\mathrm{PB}}^0. \tag{5.10}$$

Equations (2.6), (5.9) and (5.10) give four equations with unknown $\hat{\beta}_1$, $\hat{\beta}_2$, $\hat{\alpha}_3$, and $\hat{r}$. They can be reduced to a single equation for either of the first two unknowns, which can be solved using Newton's method for different values of the strain γ. Knowing these values, we use the hat versions of (2.3) and (2.4) to get

$$\hat{\alpha}_1 = \hat{\alpha}_2 = \tfrac{1}{2}(\pi - \hat{\alpha}_3), \quad \hat{d}_3 = \cos\hat{\alpha}_1 + \cos\hat{\alpha}_2 - 1. \tag{5.11}$$

The distance $\hat{D}_k$ is now determined from (2.5) which also gives $\hat{G}_3$, since $\hat{L}_3$ equals zero. Finally, $\hat{\beta}_3$, $\hat{G}_1$ and $\hat{G}_2$ are calculated from the hat versions of (2.6) and (5.8).

5.3. *Rate dependent mode I and mode II problems*

The equations that determine the prime quantities are found by substituting expansions like (2.14) into the basic equations. From (2.3) to (2.5), we get

$$d'_1 \sin\hat{\alpha}_2 + (1+\hat{d}_1)\,\alpha'_2 \cos\hat{\alpha}_2 = d'_2 \sin\hat{\alpha}_1 + (1+\hat{d}_2)\,\alpha'_1 \cos\hat{\alpha}_1, \tag{5.12}$$

$$d'_3 = d'_1 \cos\hat{\alpha}_2 - (1+\hat{d}_1)\,\alpha'_2 \sin\hat{\alpha}_2 + d'_2 \cos\hat{\alpha}_1 - (1+\hat{d}_2)\,\alpha'_1 \sin\hat{\alpha}_1, \tag{5.13}$$

$$D'_k = r'(1+\hat{d}_k)\cot\hat{\alpha}_k + \hat{r}d'_k \cot\hat{\alpha}_k - \hat{r}(1+\hat{d}_k)\,\alpha'_k \operatorname{cosec}^2\hat{\alpha}_k. \tag{5.14}$$

From (2.7) and (2.8), we get

$$A'_{\mathrm{PB}} = 4\hat{r}r'(1+\hat{d}_1)(1+\hat{d}_2)\sin\hat{\alpha}_3 + 2\hat{r}^2[d'_1(1+\hat{d}_2) + d'_2(1+\hat{d}_1)]\sin\hat{\alpha}_3 + 2\hat{r}^2(1+\hat{d}_1)(1+\hat{d}_2)\,\alpha'_3 \cos\hat{\alpha}_3 - \pi\hat{r}r' = -A'_{\mathrm{TF}}, \tag{5.15}$$

where A'_{TF} is determined from film-level viscous flow through (3.6). The correction to the thin film lengths are

$$L'_k = G'_k - D'_k. \tag{5.16}$$

The rate dependent corrections to the instantaneous shear stress and first normal stress difference follow from (4.3) and are given by

$$\left.\begin{aligned} \sigma'_{XY} &= \frac{T_0}{A}\sum_{k=1}^{3}[(d'_k\hat{L}_k + L'_k)\sin 2\hat{\beta}_k + 2\hat{L}_k\beta'_k\cos 2\hat{\beta}_k], \\ N'_1 = \sigma'_{XX} - \sigma'_{YY} &= \frac{2T_0}{A}\sum_{k=1}^{3}[(d'_k\hat{L}_k + L'_k)\cos 2\hat{\beta}_k - 2\hat{L}_k\beta'_k\sin 2\hat{\beta}_k]. \end{aligned}\right\} \tag{5.17}$$

The quantity $\hat{d}_k$ does not appear because it is non-zero only when the length L_k is equal to zero. Equations (5.12)–(5.17) are valid for all three modes.

In mode I, all three d'_k are determined from film-level viscous flow through (3.4). Using (5.12) and (5.13), we get

$$\sqrt{3}\,\alpha'_k = \left[3d'_k - \sum_{j=1}^{3} d'_j\right]. \tag{5.18}$$

The quantities r' and D'_k are calculated from (5.15) and (5.14), respectively.

To determine the corrections to the β_k, we use (2.6) and (5.4). This leads to an equation that determines β'_3,

$$[\hat{a}_1/\sqrt{3} - \hat{e}_1 + \hat{a}_2/\sqrt{3} + \hat{e}_2]\,\beta'_3 = \tfrac{4}{3}(\hat{e}_1\alpha'_2 + \hat{e}_2\alpha'_1), \tag{5.19}$$

and the other angles through $\beta'_1 = \beta'_3 + \alpha'_2$ and $\beta'_2 = \beta'_3 - \alpha'_1$. Using (5.2) and (5.3), we get the length corrections

$$\left.\begin{aligned} \sqrt{3}G'_1 = -\hat{G}_1\alpha'_2 + 2\hat{a}_1\beta'_3, \quad \sqrt{3}G'_2 = -\hat{G}_2\alpha'_1 - 2\hat{a}_2\beta'_3, \\ 2G'_3 = -G'_1 + \sqrt{3}\,\hat{G}_1\alpha'_2 + 2\hat{e}_1\beta'_3. \end{aligned}\right\} \tag{5.20}$$

As with the mode I hat problem, we give expressions for β'_k and G'_k for the special case in which we begin with an undeformed unit cell:

$$\beta'_k\hat{G}_k/a = \frac{d'_l - d'_m}{[3(4+\gamma^2)]^{\frac{1}{2}}} + \tilde{\beta}_k d'_k + \tilde{\beta}_l d'_m + \tilde{\beta}_m d'_l,$$

$$G'_k/a = -\frac{d'_k}{(4+\gamma^2)^{\frac{1}{2}}} + \tilde{G}_k d'_k + \tilde{G}_l d'_m + \tilde{G}_m d'_l, \tag{5.21}$$

where $$\tilde{\beta}_k = \frac{\gamma^2 \sin 2\psi_k}{6(4+\gamma^2)^{\frac{1}{2}}} + \tfrac{1}{6}\gamma \cos\psi_k, \quad \tilde{G}_k = \frac{2+\gamma^2 \cos 2\psi_k}{6(4+\gamma^2)^{\frac{1}{2}}} + \tfrac{1}{6}\gamma \sin\psi_k,$$

(k, l, m) are permutations of $(1, 2, 3)$, and ψ_k was defined in (5.7).

The complete expressions for the instantaneous shear stress and first normal stress difference are evaluated from (4.3) and are given by

$$\sigma_{XY} = \frac{T_0}{a}\frac{2}{\sqrt{3}}\left[\frac{\gamma}{(4+\gamma^2)^{\frac{1}{2}}} + \frac{4}{3^{\frac{1}{3}}} Ca^{\frac{2}{3}} \sum_{k=1}^{3} P_k R_k (F_k)^{\frac{5}{3}}\right],$$

$$N_1 = \frac{T_0}{a}\frac{2}{\sqrt{3}}\left[\frac{\gamma^2}{(4+\gamma^2)^{\frac{1}{2}}} + \frac{4}{3^{\frac{1}{3}}} Ca^{\frac{2}{3}} \sum_{k=1}^{3} (\gamma F_k + \cos\psi_k) P_k R_k (F_k)^{\frac{2}{3}}\right], \tag{5.22}$$

where $$F_k = \frac{1}{a}\frac{d\hat{L}_k}{d\gamma} = \frac{\gamma}{4(4+\gamma^2)^{\frac{1}{2}}} + \tfrac{1}{2}\sin\psi_k - \frac{\gamma}{4+\gamma^2}\cos\psi_k.$$

The leading-order terms, which represent the quasi-static stress, were derived by Khan & Armstrong (1986) and do not depend on the initial orientation of the foam. This isotropic material response does not carry over to other modes or to the rate-dependent terms. So in general, a monodisperse, spatially periodic foam exhibits anisotropic rheology.

In the quasi-static mode II problem discussed in §5.2, we examined the case in which $L_3 = 0$; thus, d_1' and d_2' are determined from the film-level viscous flow. The prime versions of (5.9) are

$$\left.\begin{aligned} \hat{a}_1 \beta_1' &= r' \cos\hat{\alpha}_3 + \hat{r} d_2' \cos\hat{\alpha}_3 - \hat{r}\alpha_3' \sin\hat{\alpha}_3, \\ \hat{a}_2 \beta_2' &= -r' \cos\hat{\alpha}_3 - \hat{r} d_1' \cos\hat{\alpha}_3 + \hat{r}\alpha_3' \sin\hat{\alpha}_3. \end{aligned}\right\} \tag{5.23}$$

These equations, (5.15), and the prime version of (2.6) provide four linear equations for the unknowns β_1', β_2', α_3', and r'. The quantities α_1', α_2', and d_3' are now determined from (5.12) and (5.13). The remaining quantities D_k', β_3', and G_k' are calculated from (5.14) and the prime versions of (2.6) and (5.8).

5.4. *Mode III problem*

To consider any foam orientation other than $\theta = 0$, it is necessary to examine the mode III problem. A transition from mode II to mode III occurs when the length of two thin films equals zero. Throughout this section, we assume $L_1 = L_2 = 0$, and recognize that the other cases are given by permuting indices. Setting $G_1 = D_1$ and $G_2 = D_2$ in (5.2) and (5.3) and using (2.3) and (2.5), we get

$$-G_3 = D_1 \cos\alpha_2 + a_1 = D_2 \cos\alpha_1 + a_2, \tag{5.24}$$

$$e_1 = D_1 \sin\alpha_2 = r(1+d_2)\cos\alpha_1, \tag{5.25}$$

$$-e_2 = D_2 \sin\alpha_1 = r(1+d_1)\cos\alpha_2. \tag{5.26}$$

Recognizing that $D_1 \cos\alpha_2 = D_2 \cos\alpha_1$, (5.24) simplifies to $a_1 = a_2$ and can be written,

$$\tan\beta_3 = \frac{b_{2X} - b_{1X}}{b_{1Y} - b_{2Y}}. \tag{5.27}$$

This equation determines $\hat{\beta}_3$ and also gives $\beta_3' = 0$. Combining (5.25), (5.26) and (2.4) provides an equation for r,

$$e_1 - e_2 = r(1+d_3). \tag{5.28}$$

Its solution is $$\hat{r} = \hat{e}_1 - \hat{e}_2, \quad r' = -\hat{r}d_3', \tag{5.29}$$

where $\hat{d}_3 = 0$ and d_3' is determined from film-level viscous flow.

Combining (5.25), (5.26) and (2.7) leads to equations for α_1 and α_2 in terms of known quantities,

$$\left.\begin{aligned} A_{\mathrm{PB}} &= 2re_1(1+d_3)\tan\alpha_1 - \tfrac{1}{2}\pi r^2, \\ A_{\mathrm{PB}} &= -2re_2(1+d_3)\tan\alpha_2 - \tfrac{1}{2}\pi r^2. \end{aligned}\right\} \tag{5.30}$$

Using these and the prime version of (2.9), we can determine α_1 and α_2 to $O(Ca^{\frac{2}{3}})$. Here, A_{TF} in (2.9) is just the area of thin film 3. The remaining angles β_1, β_2, and α_3 are calculated from (2.6).

Finally, d_1 and d_2 are determined from permuted versions of (2.3),

$$d_1 = (1+d_3)\frac{\sin\alpha_1}{\sin\alpha_3} - 1, \quad d_2 = (1+d_3)\frac{\sin\alpha_2}{\sin\alpha_3} - 1. \tag{5.31}$$

The quantities D_1, D_2, and G_3 are derived from (5.24) to (5.26), and D_3 is determined from (2.5).

6. Evaluation of viscometric functions

The effective viscosity and other viscometric functions for a spatially periodic foam are evaluated by averaging the instantaneous stress over time (Adler, Zuzovsky & Brenner 1985; Kraynik & Hansen 1986, 1987). Only when the structure and stress are periodic functions of strain is the appropriate choice of time interval obvious; then,

$$\bar{\boldsymbol{\sigma}} = \gamma_{\mathrm{p}}^{-1} \int_{\gamma}^{\gamma+\gamma_{\mathrm{p}}} \boldsymbol{\sigma}\, \mathrm{d}\gamma, \tag{6.1}$$

where $\bar{\boldsymbol{\sigma}}$ is the time-averaged stress and γ_{p} is the strain period. This average includes contributions from all intermediate foam structures and removes the explicit dependence on time that is associated with a spatially periodic model.

Kraynik & Hansen (1986) derived necessary conditions on the initial orientation angle θ for strain periodic response in simple shearing flow. There is an infinite set of such orientations θ_{p} which satisfy

$$\tan\theta_{\mathrm{p}} = \sqrt{3}I/(I+2J) \quad \text{with } \gamma_{\mathrm{p}} = 2(I^2+IJ+J^2)/\sqrt{3}, \tag{6.2}$$

where I and J are relatively prime integers such that $I \geqslant 0$, $J \geqslant I$, and $J > 0$; this covers all orientations $0 \leqslant \theta_{\mathrm{p}} < \frac{1}{3}\pi$.

7. Results for simple shearing flow

7.1. *Simple shearing flow: $\theta = 0$*

The case examined by Princen (1983), $\theta_{\mathrm{p}} = 0$, has the smallest strain period $\gamma_{\mathrm{p}} = 2/\sqrt{3}$. For reasons that will become clear, it is the easiest situation to analyse. To model viscous flow as quasi-steady for all times, we restrict ourselves to conditions giving continuous quasi-static solutions; this requires that

$$\frac{\sqrt{3}(4-\pi)}{14+8\sqrt{3}} < \phi < 1 - \frac{\pi}{2\sqrt{3}}, \tag{7.1}$$

or $0.9069 < \phi_{\mathrm{d}} < 0.9466$ (see figure 7). We refer to materials satisfying such continuity conditions as wet foams. In each period, there is a single transition from

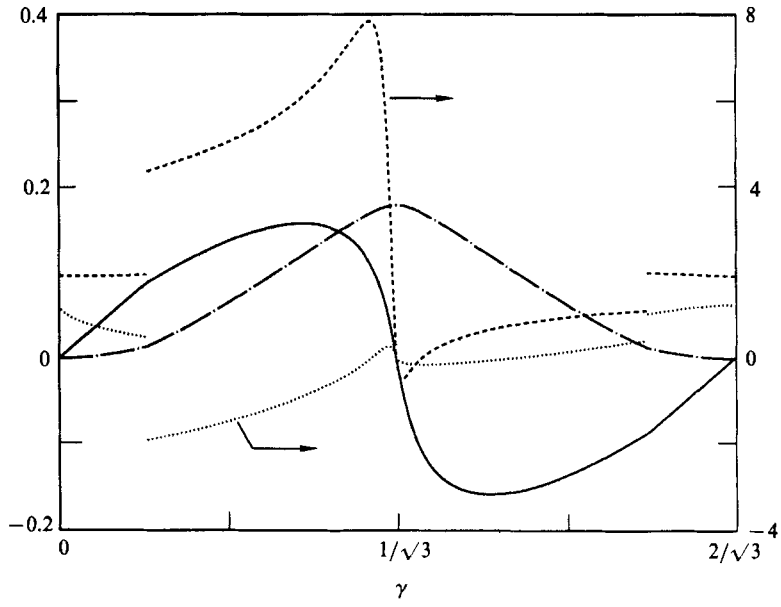

FIGURE 8. Instantaneous stress *vs.* strain for simple shear with $\theta = 0$ and $\phi = 0.07$; ——, $\hat{\sigma}_{XY}$; – – –, σ'_{XY}; —·—, $\hat{N}_1$; ..., N'_1. In all figures, the stress is scaled by T_0/a.

mode I to mode II and then back, as shown in figure 6; and, the transition strains depend on ϕ. The unit cell switches when $\gamma = 1/\sqrt{3}$.

For this particular case, both the length of each thin film and the magnitude of its withdrawal speed are symmetric about $\gamma = 1/\sqrt{3}$ and monotonic over a half period. Under these conditions, each film recedes into the Plateau border at the same thickness and speed at which it was withdrawn; therefore, the coefficients P_k and R_k that are associated with the film-level viscous flow, are also constant for film recession (Schwartz & Princen 1987; Reinelt & Kraynik 1989). The coefficient P_k has the same value as in (3.7) but $R_k = -0.8452$ (see figure 5). This appears to be unique for $\theta = 0$.

Figure 8 shows typical instantaneous shear stress functions for $\phi = 0.07$. The function $\hat{\sigma}_{XY}$ is continuous and odd about $\gamma = 1/\sqrt{3}$ (Princen 1983). Even though $\hat{\sigma}_{XY}$ is finite, it integrates to zero over the period; thus $\overline{\hat{\sigma}_{XY}} = 0$. Discontinuities in the function σ'_{XY} occur at mode transitions and reflect discontinuities in film withdrawal speed with the significant change in geometry for coalesced Plateau borders; the total number of thin films also changes at each mode transition. Although σ'_{XY} can be negative, it must integrate to a positive quantity over the cycle, $\overline{\sigma'_{XY}} > 0$, as will be discussed in §8.

Figure 8 also shows the instantaneous first normal stress difference. The function $\hat{N}_1$ is continuous, non-negative, and even about $\gamma = 1/\sqrt{3}$. It integrates to a positive value over the period; therefore, $\overline{N_1} \gg \overline{\sigma_{XY}}$, which is certainly not typical of measured viscometric functions for viscoelastic fluids such as polymer solutions and melts. The function N'_1 is also discontinuous but in contrast to $\overline{\sigma'_{XY}}$, the sign of $\overline{N'_1}$ depends on ϕ. The time-averaged stresses, which determine viscometric functions, are shown in figure 9 as functions of ϕ_d.

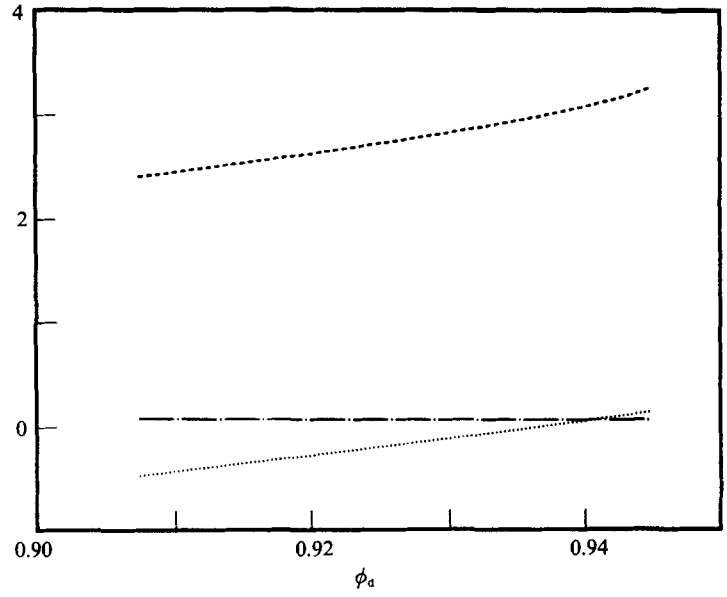

FIGURE 9. Time-averaged stress *vs.* dispersed-phase volume fraction ϕ_d for $\theta = 0$; ---, $\overline{\sigma'_{xy}}$; —·—, $\overline{N}_1$; ..., $\overline{N'_1}$.

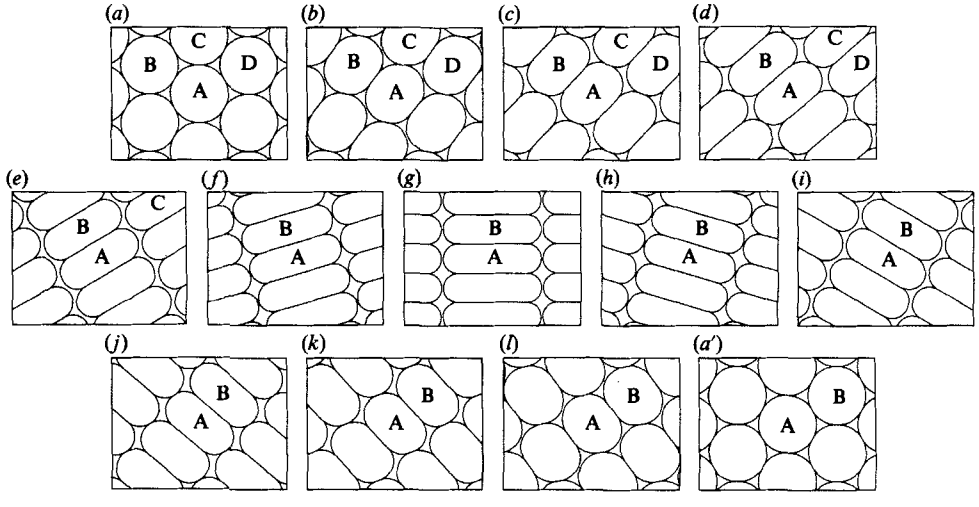

FIGURE 10. Evolution of foam structure with strain for simple shear with $\theta = \frac{1}{6}\pi$ and $\phi = 0.08$. The range of shear strain is $2\sqrt{3}$ with equal increments. Mode III structure is indicated in (*e–i*).

7.2. *Simple shearing flow:* $\theta_p \neq 0$

When $\theta_p \neq 0$, the structure of a wet foam during each cycle will involve mode III and numerous mode transitions, the number of which depends on ϕ. These cases also require evaluation of the thickness profile for each film to determine instantaneous values for P_k and R_k.

The evolution of foam structure for $\theta_p = \frac{1}{6}\pi$ ($I = J = 1$ in (7.1)) with $\phi = 0.08$ is shown in figure 10. The corresponding instantaneous stress functions are shown in figure 11. There are only four mode transitions when $\phi = 0.08$ but ten when $\phi = 0.06$.

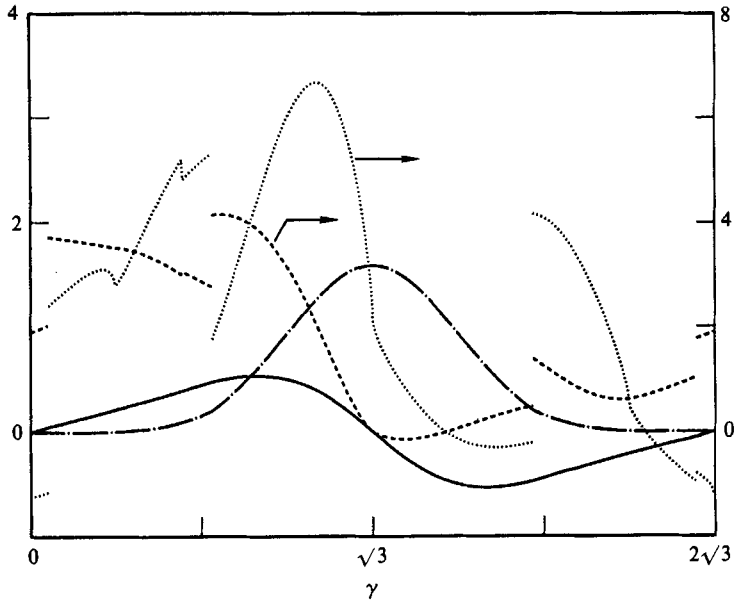

FIGURE 11. Instantaneous stress *vs.* strain for simple shear with $\theta = \frac{1}{6}\pi$ and $\phi = 0.08$; ——, $\hat{\sigma}_{XY}$; – – –, σ'_{XY}; —·—, $\hat{N}_1$; ..., N'_1.

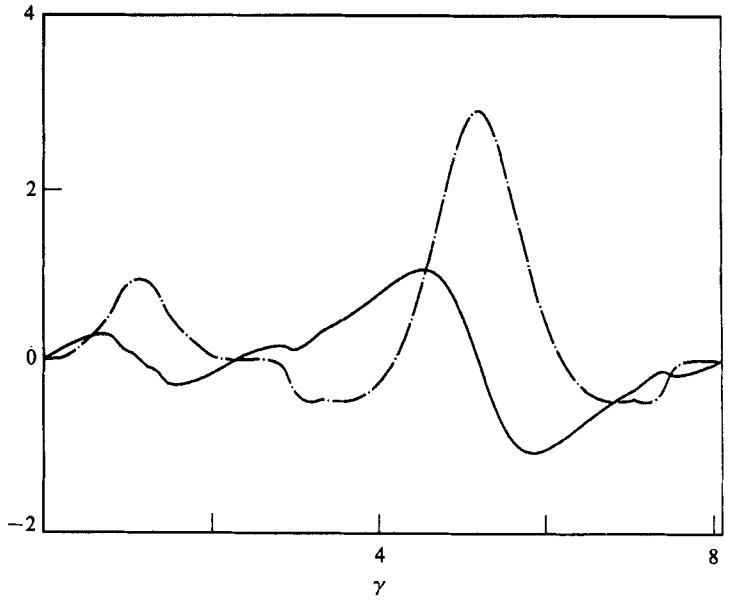

FIGURE 12. Instantaneous quasi-static stress *vs.* strain for simple shear with $\tan\theta = \sqrt{3}/5$ ($\theta \approx 0.3334$ radians) and $\phi = 0.08$; ——, $\hat{\sigma}_{XY}$; —·—, $\hat{N}_1$. Note that the normal stress difference can be negative.

We also examined the case, $\tan\theta_p = \sqrt{3}/5\,(I = 1, J = 2)$, and show in figure 12 typical instantaneous shear stress and normal stress functions to leading order. Note that in this case $\hat{N}_1$ can take on negative values. Both the length and complexity of the cycle increases with $(I^2 + IJ + J^2)$.

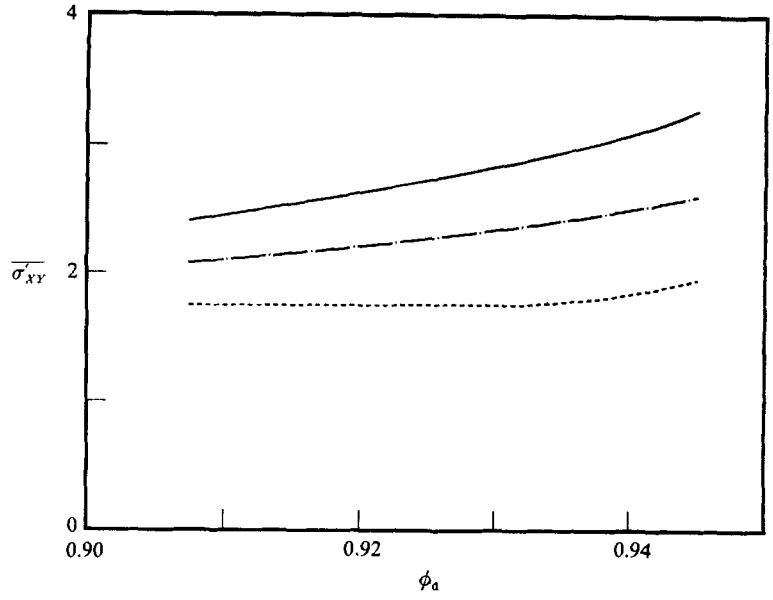

FIGURE 13. The effective viscosity coefficient $\overline{\sigma'_{XY}}$ *vs.* ϕ_d for three foam orientations: ——, $\theta = 0$; – – –, $\theta = \frac{1}{6}\pi$; and – · – · –, $\theta \approx 0.3334$ as in figure 12.

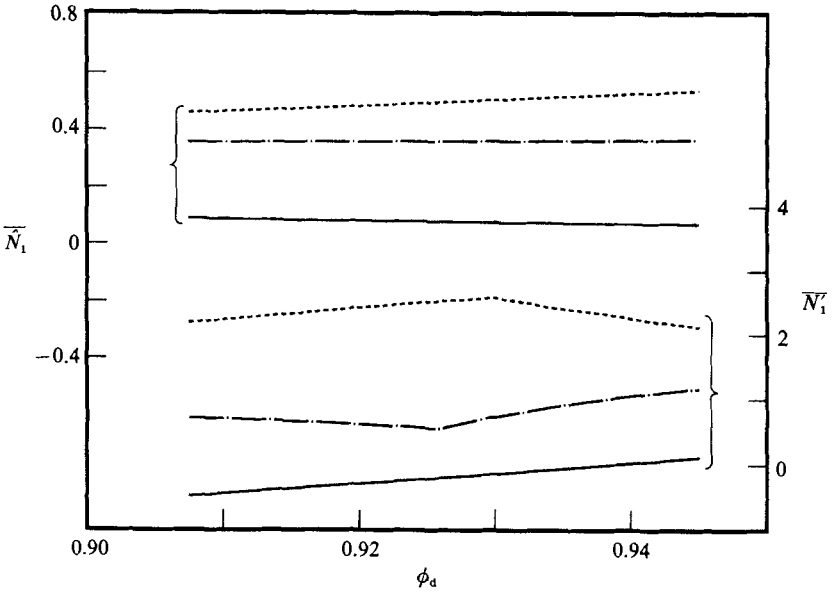

FIGURE 14. Coefficients of $\overline{N_1}$ *vs.* ϕ_d for the three foam orientations of figure 13.

7.3. *Discussion*

The effective viscosity for the foam is defined by

$$\overline{\mu_f} = \overline{\sigma_{XY}}/\dot{\gamma} = \overline{\hat{\sigma}_{XY}}/\dot{\gamma} + Ca^{\frac{2}{3}}\overline{\sigma'_{XY}}/\dot{\gamma}. \tag{7.2}$$

Because the stress is proportional to T_0/a, the last term is proportional to $\mu Ca^{-\frac{1}{3}}$.

When the quasi-static structure is continuous in strain, $\overline{\hat{\sigma}_{XY}}$ is always identically equal to zero, and such wet foams exhibit a power-law, shear-thinning viscosity

function. Figure 13 shows the dependence of the viscosity function on the liquid content and orientation of the foam. For all cases examined, the effective viscosity increases with decreasing ϕ. The quantitative results are remarkably similar for the various orientations considering the significant differences in structure evolution with strain.

Figure 14 shows that the first normal stress difference $\overline{\hat{N}_1}$ is positive for the cases examined but can increase or decrease with ϕ. The qualitative features of N_1' are even more sensitive to orientation. Thus, one cannot anticipate the behaviour of the normal stress functions for an isotropic foam with disordered structure based on the response of a monodisperse foam. The results for planar extensional flow in §9 show additional evidence of the anisotropic rheology stemming from perfectly ordered structure.

8. Macroscopic stress power

The shear stress can also be determined by evaluating the stress power for the foam. The relationship between the macroscopic stress power ζ and volume integrals of the corresponding microscopic quantities is given by Batchelor (1970). By including viscous and surface tension effects for our two-dimensional foam, we have

$$\zeta = \frac{1}{A}\int_A \boldsymbol{\nabla u}:\boldsymbol{\sigma}\,\mathrm{d}a = \Phi + \dot{W}_S, \tag{8.1}$$

where $$\Phi = \frac{1}{A}\int_A \mu\,\boldsymbol{\nabla u}:\boldsymbol{\nabla u}\,\mathrm{d}a,\ \dot{W}_S = \frac{1}{A}\int_S T\,\boldsymbol{\nabla u}:(\boldsymbol{I}-\boldsymbol{nn})\,\mathrm{d}s.$$

The term Φ represents the irreversible rate of internal energy increase by viscous dissipation; $\dot{W}_S$ is the rate at which work is done to deform interfaces. When the surface tension is constant, $\dot{W}_S = T_0\dot{S}/A$, where $\dot{S}$ is the time derivative of the total interfacial area; then and only then, $\dot{W}_S$ can be identified as the time rate of change of interfacial energy per unit volume.

The primary contributions to Φ come from the transition regions (Schwartz & Princen 1987). In the small deformation theory, Reinelt & Kraynik (1989) derived explicit formulae for Φ; their results are readily extended to large deformations and are given by

$$\Phi = \frac{6\mu}{A}\sum_{k=1}^{3} U_k^2|P_k(R_k-1)(3Ca_k)^{-\frac{1}{3}}|.$$

$$= 8\times 3^{-\frac{5}{6}}\frac{T_0}{a}\dot{\gamma}Ca^{\frac{2}{3}}\sum_{k=1}^{3} P_k(R_k-1)(F_k)^{\frac{5}{3}}. \tag{8.2}$$

This viscous dissipation term is $O(Ca^{\frac{2}{3}})$, but the surface work term involves contributions of $O(1)$ and $O(Ca^{\frac{2}{3}})$.

To evaluate $\dot{W}_S$, note that the quantity $\boldsymbol{\nabla u}:(\boldsymbol{I}-\boldsymbol{nn})$, which represents the local rate at which the interface stretches, vanishes on the inextensible thin-film interfaces where $T \neq T_0$. All creation and depletion of surface occurs in the Plateau borders where the tension is uniform and equal to the equilibrium value T_0. Knowing this, the surface integral for $\dot{W}_S$ becomes

$$\dot{W}_S = \frac{T_0}{A}\left(\dot{S}_{\mathrm{PB}} + 2\sum_{k=1}^{3}\dot{L}_k\right), \tag{8.3}$$

where S_{PB} is the time rate of change of surface area in the Plateau border. The summation accounts for convection of interface at speed $U_k = \dot{L}_k$ from the Plateau

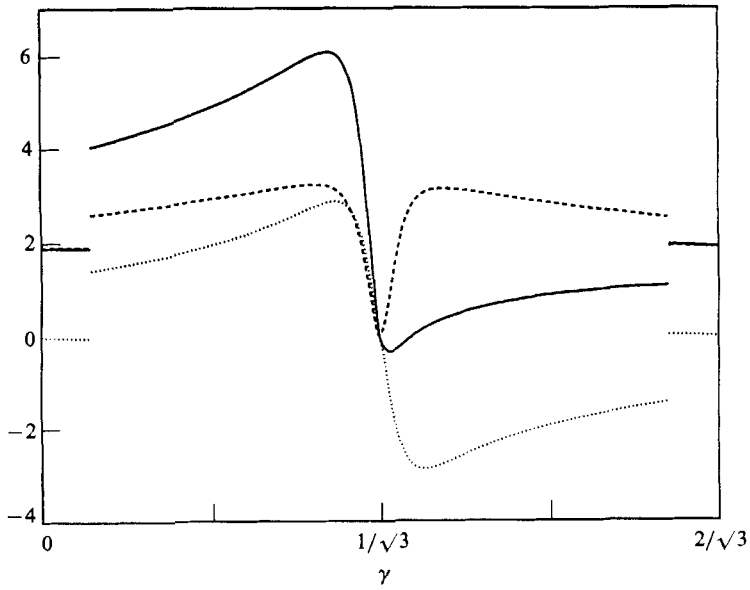

FIGURE 15. Comparison between ——, σ'_{XY}; – – –, Φ, and ..., $\dot{W}'_S$ for $\theta = 0$ and $\phi = 0.08$. The surface work $\dot{W}'_S$ integrates to zero over the cycle. The stress–power terms have dimensions of $(T_0/a)\dot{\gamma}Ca^{\frac{2}{3}}$.

border, which is not a material surface. Reinelt & Kraynik (1989) evaluated $\dot{W}_S$ explicitly for small deformations and showed that it involves finite contributions of $O(1)$ and $O(Ca^{\frac{2}{3}})$.

One can use (8.3) to show that $\dot{W}_S$ integrates to zero over a cycle because, to leading order, $S_{\rm PB}$ and L_k are continuous functions of time for a wet foam. As a consequence, the effective foam viscosity can be determined from the average value of the positive semidefinite quantity Φ. In figure 15 we compare Φ and σ'_{XY} for $\theta = 0$ and $\phi = 0.08$. The difference between these two functions determines $\dot{W}'_S$, the $O(Ca^{\frac{2}{3}})$ contribution to $\dot{W}_S$, which is also shown.

9. Planar extensional flow

The theoretical framework developed in previous sections carries over to planar extensional deformations for which (2.1) is replaced by

$$\boldsymbol{b}_k = (b^0_{kX}\,\mathrm{e}^{+\epsilon}, b^0_{kY}\,\mathrm{e}^{-\epsilon}), \tag{9.1}$$

where ϵ is the Henky strain. As in simple shear, the structure and stress for deformations of an equilibrium foam in mode I are described by analytical forms. Omitting the derivations, the film variables are given by

$$\hat{\beta}_k = \beta^0_k, \quad \hat{G}_k/a = \tfrac{1}{2}\cosh\epsilon + \cos 2\beta^0_k \sinh\epsilon,$$

$$G'_k/a = -\frac{d'_k}{2\cosh\epsilon} + \tilde{G}_k d'_k + \tilde{G}_l d'_m + \tilde{G}_m d'_l,$$

$$\beta'_k \hat{G}_k/a = \frac{d'_l - d'_m}{2\sqrt{3}\cosh\epsilon} + \tilde{\beta}_k d'_k + \tilde{\beta}_l d'_m + \tilde{\beta}_m d'_l, \tag{9.2}$$

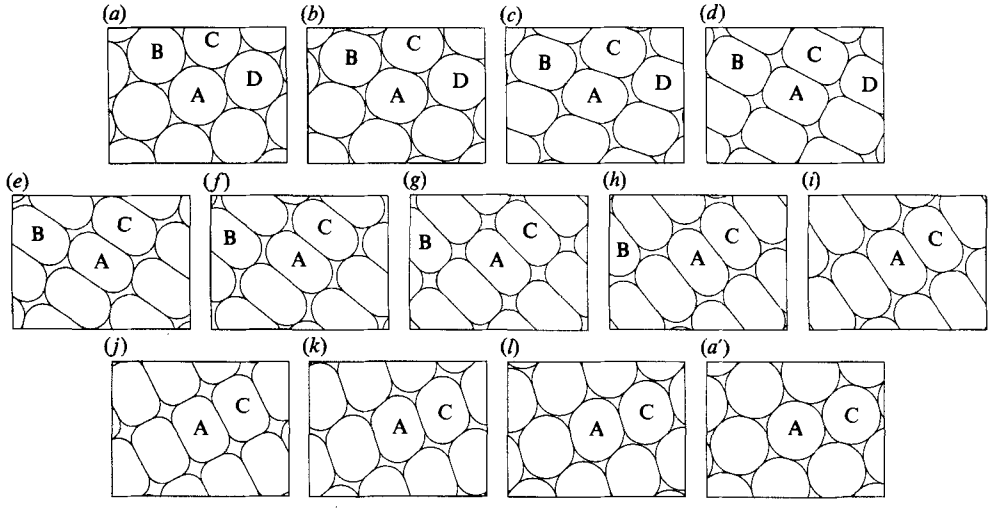

FIGURE 16. Evolution of foam structure with strain for planar extension with $\theta = \frac{1}{12}\pi$ and $\phi = 0.08$. The range of Henky strain is 1.3170 with equal increments.

where
$$\tilde{G}_k = \frac{1+\cos 2\beta_k^0 \sinh 2\epsilon - 2\cos 4\beta_k^0 \sinh^2 \epsilon}{6\cosh \epsilon},$$

$$\tilde{\beta}_k = \frac{-\sin 2\beta_k^0 \sinh 2\epsilon - 2\sin 4\beta_k^0 \sinh^2 \epsilon}{6\cosh \epsilon},$$

and (k, l, m) are permutations of $(1, 2, 3)$. The instantaneous tensile stress and shear stress are given by

$$\left.\begin{aligned} \sigma_{XX} - \sigma_{YY} &= \frac{T_0}{a}\frac{4}{\sqrt{3}}\left[\sinh \epsilon + \frac{2Ca^{\frac{2}{3}}}{3^{\frac{1}{3}}}\sum_{k=1}^{3} P_k R_k (F_k)^{\frac{5}{3}}\right], \\ \sigma_{XY} &= \frac{T_0}{a}\frac{4Ca^{\frac{2}{3}}}{3^{\frac{5}{3}}\cosh \epsilon}\sum_{k=1}^{3} P_k R_k (F_k)^{\frac{2}{3}} \sin 2\beta_k^0, \end{aligned}\right\} \tag{9.3}$$

where
$$F_k = \tfrac{1}{2}\sinh \epsilon + \cos 2\beta_k^0 \cosh \epsilon,$$

and the capillary number is based on the extension rate, $Ca = \mu a\dot{\epsilon}/T_0$.

The material functions for steady planar extensional flow can also be evaluated using the methods developed in previous sections. Again, there exists an infinite set of initial orientations for which response is strain periodic. The θ_p and ϵ_p are given by

$$\tan 2\theta_p = \sqrt{3}\frac{1-K^2+(I+K)^2}{1+K^2+(I-K)^2}, \quad \exp(\epsilon_p) = -I + \frac{2K}{1-\sqrt{3}\tan \theta_p}, \tag{9.4}$$

where
$$K = \frac{1+2IJ+I^2}{J-I}.$$

Here I and J are the relatively prime integers, $I \geqslant 0, J > 0$, for which K is also an integer. The shortest period is given by $I = 0, J = 1$ where $\theta_p = \frac{1}{12}\pi$ and $\epsilon_p \approx 1.3170$. The corresponding variation of structure and stress with strain is shown in figures 16 and 17, respectively, for $\phi = 0.07$.

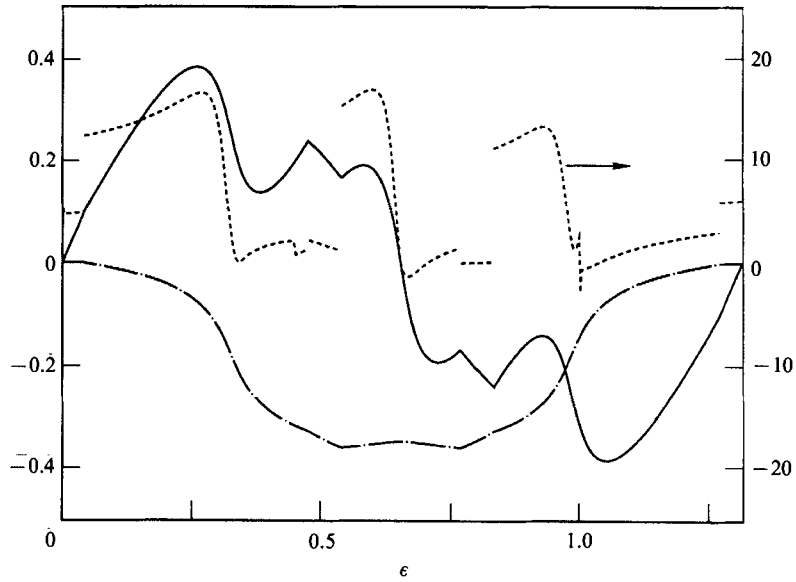

FIGURE 17. Instantaneous stress *vs.* Henky strain for planar extension with $\theta = \frac{1}{12}\pi$ and $\phi = 0.08$; ——, $\hat{\sigma}_{XX} - \hat{\sigma}_{YY}$; – – –, $\sigma'_{XX} - \sigma'_{YY}$; —·—, $\hat{\sigma}_{XY}$.

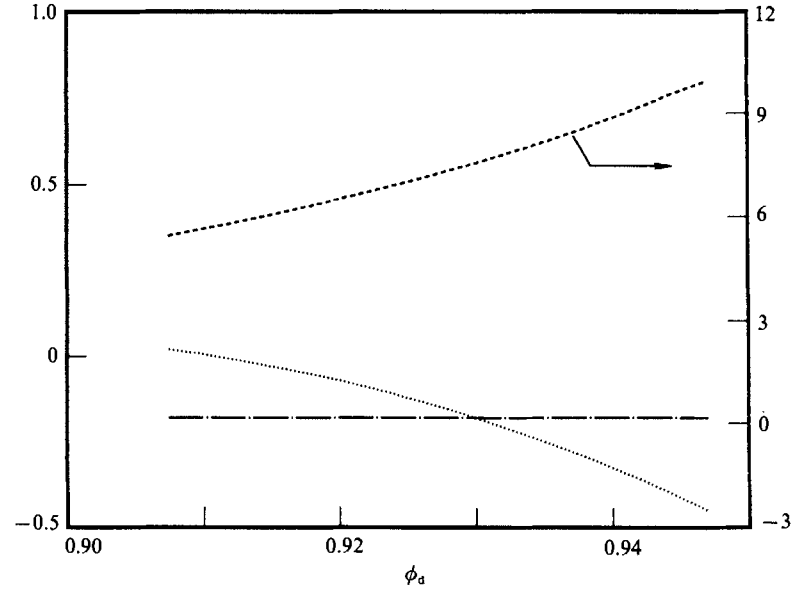

FIGURE 18. Time-averaged stress *vs.* dispersed-phase volume fraction ϕ_d for planar extension with $\theta = \frac{1}{12}\pi$; ----, $\overline{\sigma'_{XX}} - \overline{\sigma'_{YY}}$; —·—, $\overline{\hat{\sigma}_{XY}}$; · · · · · ·, $\overline{\sigma'_{XY}}$. The shear stress $\overline{\sigma_{XY}}$ would be equal to zero for an isotropic material.

Again, by restricting the range of ϕ to give continuous quasi-static solutions, we can evaluate the planar extensional viscosity

$$\overline{\eta_t} = (\overline{\sigma_{XX}} - \overline{\sigma_{YY}})/\dot{\epsilon} = (\overline{\sigma'_{XX}} - \overline{\sigma'_{YY}})/\dot{\epsilon}. \tag{9.5}$$

We have used the fact that $(\overline{\hat{\sigma}_{XX}} - \overline{\hat{\sigma}_{YY}})$ is identically equal to zero for the wet foams under consideration; thus, $\overline{\eta_t}$ is proportional to $\mu Ca^{-\frac{1}{3}}$. Figure 18 indicates that the

variation of extensional viscosity with ϕ_d is qualitatively similar to the shear viscosity. Also shown is the average shear stress $\overline{\hat{\sigma}_{XY}}$, which is finite, indicating that the material response is not isotropic throughout the entire cycle. By contrast, (9.3) shows that the quasi-static response is isotropic for deformations of an equilibrium foam in mode I (Khan & Armstrong 1986).

10. Concluding remarks

In this analysis we determine the rate-dependent rheology for slow steady shearing flow of a model wet foam with inextensible thin-film interfaces. The viscosity functions for simple shear and planar extension exhibit the same power-law dependence on strain rate and show no evidence of a yield stress. This time-averaged behaviour seems to contradict the solid-like response for small strains, where, for example, in simple shear $\hat{\sigma}_{XY}$ is finite and its local maximum has been identified as a yield stress. Not only the value but the existence of a yield stress can depend on whether the definition is based on instantaneous or time-averaged conditions.

Even though the instantaneous structure and stress exhibit strong anisotropy during steady simple shearing flow, the predicted foam viscosity $\overline{\mu_f}$ always increases with decreasing liquid content and is relatively insensitive to the initial foam orientations examined. The rate-dependent rheology exhibited by our model stems from viscous flow induced by film withdrawal from Plateau borders. Plateau-border coalescence and separation determines the number of thin films; when these processes occur depends on the liquid content of the foam. Dependence of viscosity on liquid volume fraction follows. By contrast, small deformations do not involve Plateau-border coalescence and the corresponding rate-dependent contributions to the stress do not depend on liquid content. Therefore, the 'extensional viscosity' obtained by Schwartz & Princen (1987) in their *ad hoc* calculation does not depend on liquid volume fraction. In addition, the initial foam orientation that they consider is not strain periodic and the tensile stress increases without bound for steady planar extensional flow.

Because viscous flow in the bubbles has been neglected, our results do not apply when the dispersed-phase viscosity μ_0 is too large. To quantify this, assume that the dispersed phase contributes a rate-dependent term of $O(\mu_0 \dot{\gamma})$ to the stress, which can be compared to the term of $O(T_0 Ca^{\frac{2}{3}}/a)$ for the film-level viscous flow considered here. If the thin-film interfaces remain inextensible, it follows that dispersed-phase flow can be neglected when

$$\mu_0/\mu \ll Ca^{-\frac{1}{3}}. \tag{10.1}$$

Thus, the thin-film flow determines the rate-dependent rheology even though the volume fraction of the dispersed phase is larger and its viscosity may be somewhat larger.

Although quantitative agreement cannot be expected, it is worth comparing our results with recent, careful measurements by Princen & Kiss (1989) of shear viscosity for concentrated emulsions. Their data can be represented by (7.2) with rate dependence of $O(Ca^{\frac{1}{3}})$ instead of $O(Ca^{\frac{2}{3}})$. The data indicate that $\overline{\hat{\sigma}_{XY}}$ is finite, so the emulsions exhibit a yield stress. This is consistent with the fact that their 'three-dimensional' emulsions cannot be considered 'wet' because $0.833 < \phi_d < 0.976$. Also consistent with our analysis, their measured $\overline{\sigma'_{XY}}$ decreases with increasing liquid content. The discrepancy in the exponent on Ca can be attributed to many things. Princen & Kiss suggest neglect of disjoining-pressure effects. In addition, we note that the assumption of inextensible thin-film interfaces was not investigated

experimentally. Moreover, μ_0 and μ are 49 and 1.53 mPa s, respectively, for the emulsions studied, and the viscosity data correspond to Ca ranging from 10^{-6} to 10^{-4}. Under these conditions, (10.1) is violated and drop viscosity may be important.

Each feature of the idealized structure – taken to be two-dimensional, monodisperse, and spatially periodic – is a significant factor in the tractability of this analysis. Each of these idealizations compromises to a greater or lesser degree, the structure of a real foam, which is three-dimensional, polydisperse, and disordered.

The geometrical constraints imposed here retain some essential physical features of foams, such as thin films and Plateau borders. Also retained are essential microrheological mechanisms, such as coalescence and separation of Plateau borders, which lead to neighbour switching. Many features of foam rheology predicted here are in qualitative accord with experiment. Other features are physically implausible for obvious reasons; for example and perhaps foremost, the macroscopic response of a monodisperse, spatially periodic foam reflects the interaction of individual bubbles with identical neighbours. During flow, this leads to strong dependence of structure and stress on strain and initial orientation.

A highly disordered two-dimensional foam should exhibit isotropic rheological response and reduced fluctuations in stress with strain. The coalescence and separation of Plateau borders will no longer occur simultaneously throughout the foam. Extending the current analysis to disordered structure shows promise. The simulation methods developed by Weaire & Kermode (1983, 1984) and Weaire & Fu (1988) will require modification for finite liquid content and the corresponding structural complexity.

By restricting this theory to wet foams, the film-level viscous flow can be considered quasi-steady and is conveniently described by asymptotic results. When the foam contains little liquid, solutions for structure lose continuity with strain. This leads to abrupt separation of Plateau borders and fast film-level flow. The corresponding large capillary number film withdrawal problem has not been analysed. It is required to extend this theory to small liquid volume fractions where the foam viscosity function will exhibit a yield stress.

There has been progress over the past decade, but it is clear that the rheology of foams and concentrated emulsions will continue to provide significant challenge to experimentalists and theorists.

This work was performed at Sandia National Laboratories and supported by the US Department of Energy under contract DE-AC04-76DP00789. D. A. R. would like to thank the Applied Mathematics Department and Fluid and Thermal Sciences Department at Sandia National Laboratories for providing research funding during the summer of 1988.

REFERENCES

Adler, P. M. & Brenner, H. 1985 Spatially periodic suspensions of convex particles in linear shear flows. I. Description and kinematics. *Intl J. Multiphase Flow* **11**, 361–385.

Adler, P. M., Zuzovsky, M. & Brenner, H. 1985 Spatially periodic suspensions of convex particles in linear shear flows. II. Rheology. *Intl J. Multiphase Flow* **11**, 387–417.

Batchelor, G. K. 1970 The stress system in a suspension of force-free particles. *J. Fluid Mech.* **41**, 545–570.

Bretherton, F. P. 1961 The motion of long bubbles in tubes. *J. Fluid Mech.* **10**, 166–188.

Cox, R. G. 1969 The deformation of a drop in a general time-dependent fluid flow. *J. Fluid Mech.* **37**, 601–623.

Flumerfelt, R. W. 1980 Effects of dynamic interfacial properties on drop deformation and orientation in shear and extensional flow fields. *J. Colloid Interface Sci.* **76**, 330–349.

FRANKEL, N. A. & ACRIVOS, A. 1970 The constitutive equation for a dilute emulsion. *J. Fluid Mech.* **44**, 65–78.

KELVIN, LORD (THOMPSON, W.) 1887 On the division of space with minimum partitional area. *Phil. Mag.* **24**, 503–514.

KHAN, S. A. 1985 Rheology of large gas fraction liquid foams. PhD thesis, MIT, Cambridge.

KHAN, S. A. & ARMSTRONG, R. C. 1986 Rheology of foams: I. Theory for dry foams. *J. Non-Newtonian Fluid Mech.* **22**, 1–22.

KHAN, S. A. & ARMSTRONG, R. C. 1987 Rheology of foams: II. Effects of polydispersity and liquid viscosity for foams having gas fraction approaching unity. *J. Non-Newtonian Fluid Mech.* **25**, 61–92.

KHAN, S. A. & ARMSTRONG, R. C. 1989 Rheology of foams: IV. Effect of gas volume fraction. *J. Rheol.* **33**, 881–911.

KRAYNIK, A. M. 1988 Foam flows. *Ann. Rev. Fluid Mech.* **20**, 325–357.

KRAYNIK, A. M. & HANSEN, M. G. 1986 Foam and emulsion rheology: a quasistatic model for large deformations of spatially periodic cells. *J. Rheol.* **30**, 409–439.

KRAYNIK, A. M. & HANSEN, M. G. 1987 Foam rheology: a model of viscous phenomena. *J. Rheol.* **31**, 175–205.

LANDAU, L. & LEVICH, B. 1942 Dragging of a liquid by a moving plate. *Acta Physicochim. URSS* **17**, 42–54.

LYKLEMA, J., SCHOLTEN, P. C. & MYSELS, K. J. 1965 Flow in thin liquid films. *J. Phys. Chem.* **69**, 116–123.

MYSELS, K. J. & COX, M. C. 1962 An experimental test of Frankel's law of film thickness. *J. Colloid Interface Sci.* **17**, 136–145.

MYSELS, K. J., SHINODA, K. & FRANKEL, S. 1959 *Soap Films: Studies of Their Thinning.* Pergamon.

PACETTI, S. D. 1985 *Structural modeling of foam rheology.* MS thesis, University of Houston, Texas.

PARK, C.-W. & HOMSY, G. M. 1984 Two-phase displacement in Hele-Shaw cells: theory. *J. Fluid Mech.* **139**, 291–308.

PRINCEN, H. M. 1983 Rheology of foams and highly concentrated emulsions I. Elastic properties and yield stress of a cylindrical model system. *J. Colloid Interface Sci.* **91**, 60–75.

PRINCEN, H. M. & KISS, A. D. 1989 Rheology of foams and highly concentrated emulsions: IV. An experimental study of the shear viscosity and yield stress of concentrated emulsions. *J. Colloid Interface Sci.* **128**, 176–187.

REINELT, D. A. & KRAYNIK, A. M. 1989 Viscous effects in the rheology of foams and concentrated emulsions. *J. Colloid Interface Sci.* **132**, 491–503.

SCHOWALTER, W. R., CHAFFEY, C. E. & BRENNER, H. 1968 Rheological equation of a dilute emulsion. *J. Colloid Interface Sci.* **26**, 152–160.

SCHOWALTER, W. R. 1978 *Mechanics of Non-Newtonian Fluids.* Pergamon.

SCHWARTZ, L. W. & PRINCEN, H. M. 1987 A theory of extensional viscosity for flowing foams and concentrated emulsions. *J. Colloid Interface Sci.* **118**, 201–211.

TAYLOR, G. I. 1932 The viscosity of a fluid containing small drops of another fluid. *Proc. R. Soc. Lond.* A **138**, 41–48.

TAYLOR, G. I. 1954 The two coefficients of viscosity for an incompressible fluid containing air bubbles. *Proc. R. Soc. London* A **226**, 34–39.

TELETZKE, G. F., DAVIS, H. T. & SCRIVEN, L. E. 1988 Wetting hydrodynamics. *Rev. Phys. Appl.* **23**, 989–1007.

WEAIRE, D. & FU, T.-L. 1988 The mechanical behavior of foams and emulsions. *J. Rheol.* **32**, 271–283.

WEAIRE, D., FU, T.-L. & KERMODE, J. P. 1986 On the shear elastic constant of a two-dimensional froth. *Phil. Mag.* B **54**, L39–L43.

WEAIRE, D. & KERMODE, J. P. 1983 Computer simulation of a two-dimensional soap froth. I. Method and motivation. *Phil. Mag.* B **48**, 245–259.

WEAIRE, D. & KERMODE, J. P. 1984 Computer simulation of a two-dimensional soap froth. II. Analysis of results. *Phil. Mag.* B **50**, 379–395.